

pubs.acs.org/acscatalysis Research Article

Explaining Kinetic Trends of Inner-Sphere Transition-Metal-Ion Redox Reactions on Metal Electrodes

Harsh Agarwal, Jacob Florian, Daniel Pert, Bryan R. Goldsmith, and Nirala Singh*



Cite This: ACS Catal. 2023, 13, 2223-2233



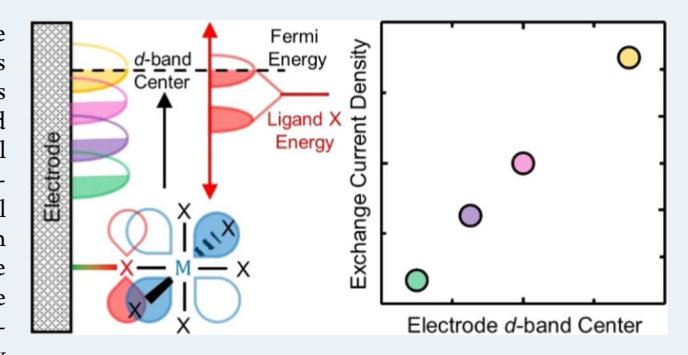
ACCESS I

III Metrics & More

Article Recommendations

s Supporting Information

ABSTRACT: Transition-metal ions regularly undergo charge transfer (CT) by directly interacting with electrodes, and this CT governs the performance of devices for numerous applications like energy storage and catalysis. These CT reactions are deemed inner sphere because they involve direct formation of a chemical bond between the electrode and the metal ion. Predicting innersphere CT kinetics on electrodes using simple physicochemical descriptors would aid the design of electrochemical systems with improved kinetics. Herein, we report that the average energy of the d electrons (i.e., d-band center) of a transition-metal electrode rationalizes the kinetic trends of inner-sphere CT of transition-metal ions. We demonstrate that V^{2+}/V^{3+} , an important redox



reaction for flow batteries, is an inner-sphere reaction and that the kinetic parameters correlate with the adsorption strength of the vanadium intermediate on Au, Ag, Cu, Bi, and W electrodes, with W being the most active electrode reported to date. We show that the adsorption strength of the vanadium intermediate linearly correlates with the d-band center such that the d-band center serves as a simple descriptor for the V^{2+}/V^{3+} kinetics. We extract kinetic data from the literature for four other inner-sphere CT reactions of metal ions involving Cr-, Fe-, and Co-based complexes to show that the d-band center also linearly correlates with kinetic trends for these systems. The d-band center of the electrode is a general descriptor for heterogeneous inner-sphere CT because it correlates with the adsorption strength of the metal-ion intermediate. The d-band center descriptor is analogous to the d-electron configuration of metal ions serving as a descriptor for homogeneous inner-sphere CT because the d-electron configuration controls bond strengths of intermediate metal-ion complexes.

KEYWORDS: energy storage, redox kinetics, charge transfer, electrocatalysis, transition-metal ions, vanadium

1. INTRODUCTION

Charge transfer (CT) reactions involving transition-metal ions are critical in many natural phenomena and applications, including photosynthesis, ^{1,2} biological systems, ^{3–5} electrodeposition, ^{6–8} corrosion, ^{9–11} chemical sensors, ^{3,12} and energy storage. ^{13,14} In redox flow batteries and metal-air batteries, CT kinetics of metal ions at an electrode are often a limiting factor in device performance. For example, the round-trip electrical efficiencies of vanadium redox flow batteries (VRFBs) are reduced in part due to slower V2+/V3+ charge transfer preventing VRFBs from operating at high current densities, increasing their capital costs. 15-17 Although Bi, 18-22 Ag, 23 Sb,²⁴ W,²⁵ Cu,²⁶ and Sn²⁷ on carbon supports have shown improved kinetics for the V^{2+}/V^{3+} reaction, there is little understanding of the reason behind this kinetic enhancement and whether there are any trends in the kinetics with electrode properties. Various challenges have prevented a fair comparison of activity among electrodes for V²⁺/V³⁺ and several other transition-metal-ion redox couples, 28-30 including the absence of reaction rates normalized by the electrochemically active surface area (ECSA), differences in experimental techniques

(cyclic voltammetry at different scan rates, CT resistance at different voltages) and testing conditions (mass transfer limitations), and not capturing the effect of metal deposition and functionalization on the properties of the carbon support. In this work, by addressing the above challenges, we show that V^{2+}/V^{3+} redox kinetics vary by several orders of magnitude across electrodes. We demonstrate that the d-band center of the electrode linearly correlates with kinetics for the V^{2+}/V^{3+} reaction on a series of metal electrodes, and similar correlations hold for four other inner-sphere reactions at electrodes involving transition-metal ions.

The large catalytic effect of the electrode on the kinetics of heterogeneous inner-sphere CT (het-CT) reactions of transition-metal ions is poorly understood. Because of the

Received: November 20, 2022 Revised: December 29, 2022



importance of the electrode in het-CT reactions, developing an understanding of what electrode properties control rates would aid the design of more active materials for this diverse range of applications. Inner-sphere CT of transition-metal ions at electrodes involves formation of a chemical bond between the electrode and the metal ion, typically through a bridging ligand. The bridging ligand mediates the electron transfer between the electrode and metal ion. Bridging ligands are typically molecules containing p-block elements like C, N, O, P, S, and halides.^{31–33} The exchange current densities (i_0) or rate constants (k) vary by several orders of magnitude on different electrodes for het-CT. $^{34-37}$ Changes of this magnitude in i_0 and k cannot be attributed solely to doublelayer changes at the electrode-electrolyte interface, so the electronic structure of the electrode must have an effect on the energies of intermediate steps. 38,39 The i_0 and k have been shown to correlate with electrode properties such as point of zero charge, 40,41 work function, 40,42 electronegativity, 42,43 and polarizability for inner-sphere CT reactions of Fe²⁺/Fe³⁺ complexes; 44 however, there is a lack of physical understanding of why these properties correlate with kinetics and how universally these correlations hold.

We hypothesize that the large catalytic effect of the electrode (i.e., orders of magnitude changes in i_0 and k) in het-CT is because of the electrode's influence on the adsorption energy of the intermediate. We denote this intermediate species as *[X-M], where * represents the electrode surface and X is the bridging ligand through which metal ion M adsorbs. We have previously shown that for the V^{2+}/V^{3+} reaction on carbon electrodes, the i_0 , apparent activation energy (E_a) , and apparent frequency factor are related to the adsorption strength of the vanadium intermediate (*[X-V³⁺]) and a three elementary step reaction mechanism involving adsorption, electron transfer, and desorption is able to explain the kinetic trends. 32,33 Herein, we investigate whether this relationship between V^{2+}/V^{3+} kinetics and adsorption strength of the metal ion extends to metal electrodes and whether an electrode property exists that can describe the trends in kinetics for het-CT reactions of transition-metal ions.

In this work, we measure the V^{2+}/V^{3+} kinetics on five different metal electrodes in sulfuric acid and compute the adsorption energies of the vanadium intermediate on these electrodes. We find that $V^{2+}/V^{3+}i_0$ varies by several orders of magnitude across electrodes and W has the highest i_0 of any reported electrocatalyst for V²⁺/V³⁺. We demonstrate that the kinetics follows a trend with the adsorption energy of the vanadium intermediate. Furthermore, we show that V^{2+}/V^{3+} kinetics linearly correlates with the d-band center of the different electrodes. We demonstrate that the d-band center controls the kinetics by changing the adsorption strength of the metal-ion CT intermediate. We extend this analysis to show that the d-band center also linearly correlates with the kinetics of het-CT reactions involving Cr-, Fe-, and Co-based complexes on different electrodes reported in the literature. The d-band correlation is stronger than those of other electrode properties proposed to explain kinetic trends.

2. RESULTS

2.1. V^{2+}/V^{3+} Reaction Kinetics on Metal Electrodes. We address the challenges highlighted in the Introduction section that have prevented a fair comparison of V^{2+}/V^{3+} kinetics on different electrodes by: (i) using unsupported

metals as electrodes in a single electrolyte to ensure any

changes in activity are solely from the metal itself, (ii) measuring ECSA normalized kinetics, and (iii) measuring kinetic parameters using steady-state current measurements and CT resistance at open-circuit voltages using a rotating disk electrode that provides control over mass transfer limitations. Mitigating these challenges allows us to understand the V^{2+}/V^{3+} reaction mechanism and identify physicochemical descriptors that explain kinetic trends.

We measure the V²⁺/V³⁺ kinetic parameters on Au, Ag, Cu, Bi, and W metal electrodes in H₂SO₄ to isolate the effect of the electrode on charge transfer. We choose these metal electrodes for our analysis because of their varying d-band center and other electronic properties like work function, polarizability, and electronegativity. The remaining metals in the d-block are unstable at the V^{2+}/V^{3+} redox potential, radioactive, or are good electrocatalysts for hydrogen evolution reaction (HER) making it difficult to measure V²⁺/V³⁺ kinetics. Even though Bi is not a d-block element, we include Bi for our analysis because Bi is the electrocatalyst used in the best-performing VRFB reported to date and serves as a benchmark for comparing the kinetic performance of other metal electrocatalysts.⁴⁵ Because V³⁺ interacts with anions present in the electrolyte and often forms complexed species, we use the same electrolyte to ensure the structure of reacting vanadium ions remains unchanged and the role of the metal electrode on V^{2+}/V^{3+} redox kinetics is isolated.^{32,33,46} We have shown previously that V²⁺ exists as $[V(H_2O)_6]^{2+}$ and V^{3+} exists as a mixture of $[V(H_2O)_5SO_4]^{+}$ and $[V(H_2O)_6]^{3+}$ in H_2SO_4 . 33,46

We measure the ECSA to ensure normalized intrinsic V^{2+} V³⁺ kinetics on Au, Ag, Cu, Bi, and W metal electrodes. We determine the ECSA of Au using Cu underpotential deposition (UPD) (Figure S1) and the ECSA of Ag and Cu using Pb UPD (Figure S2). We observe that Cu and Pb UPD do not occur on Bi and W. To our knowledge, there is not any other UPD technique previously shown to estimate ECSA for Bi and W. A previous study used HER currents to determine the ECSA of W electrodes; however, it is unclear if the measured HER currents were mass-transfer limited, and the roughness of the W electrodes was not considered.⁴⁷ We measure the ECSA of Bi (Figures S3 and S4) and W (Figures S5 and S6) electrodes by determining the HER current at a fixed voltage on our disk electrode and normalizing to the HER current on Bi and W electrodes deposited to have a roughness factor of one. We ensure that the HER currents are not mass transfer limited by operating at sufficiently high rotation or stir rates where the current is independent of mass transfer. This is the first time that HER current is used to measure ECSA of Bi electrodes, to our knowledge. The details of the ECSA measurement of the metal electrodes are described in the Supporting Information.

We evaluate the i_0 , Tafel slopes, $E_{\rm a}$, and apparent frequency factors for the V²⁺/V³⁺ reaction on Au, Ag, Cu, Bi, and W electrodes using steady-state current measurements (Tafel method) and impedance measurements (CT resistance method). We record the steady-state measurements at different rotation rates for a range of overpotentials using a rotating disk electrode setup, and use Koutecky–Levich analysis to deconvolute the contributions of kinetic and diffusive current (Figure S7).⁴⁸ The kinetic currents of the oxidation reaction are used to estimate i_0 and Tafel slopes using the Tafel equation for all metal electrodes except W. We use the Butler–Volmer equation instead of the Tafel equation to estimate i_0 on W because the limiting currents are reached at low over-

ACS Catalysis pubs.acs.org/acscatalysis Research Article

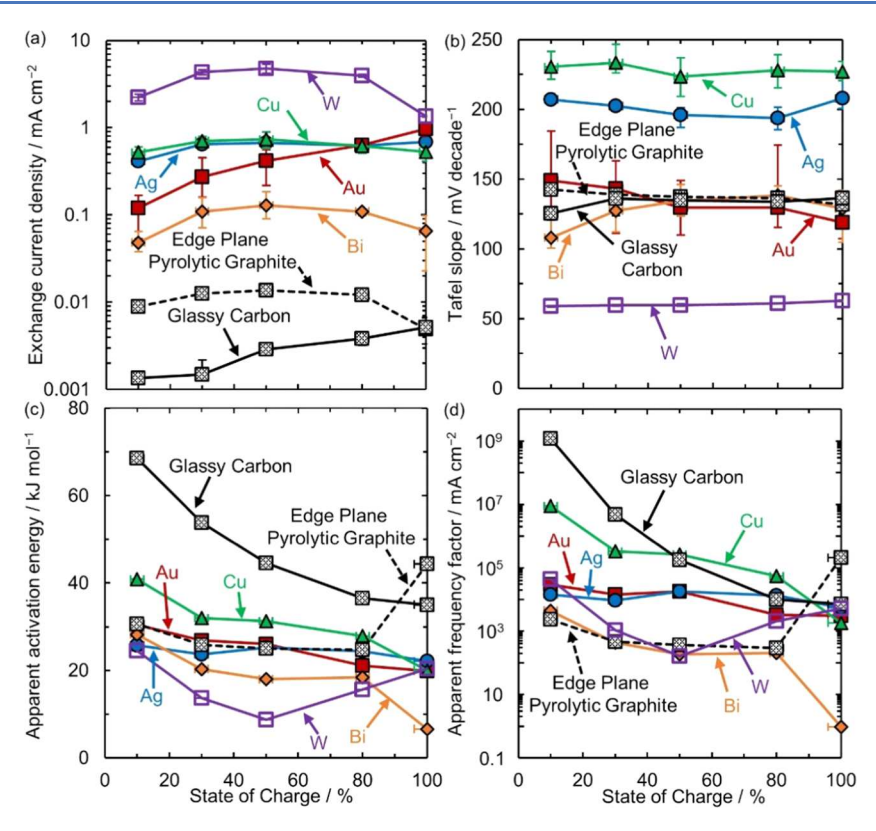


Figure 1. Kinetic parameters for the V^{2^+}/V^{3^+} reaction on metal and carbon electrodes. (a) Exchange current densities (i_0) from the Tafel method at room temperature $(T=23.3 \, ^{\circ}\text{C})$, (b) Tafel slopes at $T=23.3 \, ^{\circ}\text{C}$, (c) apparent activation energies (E_a) , and (d) apparent frequency factors as a function of state of charge for V^{2^+}/V^{3^+} reaction on Au, Ag, Cu, Bi, and W metal electrodes and edge plane pyrolytic graphite (EPPG) and glassy carbon (GC) electrodes. The E_a and apparent frequency factors are evaluated using i_0 at T=23.3, 30.0, 35.0, and 40.0 $^{\circ}\text{C}$ for all metals except W. We use i_0 at T=5.0, 10.0, 15.0, and 23.3 $^{\circ}\text{C}$ to evaluate E_a and apparent frequency factors for W because of the difficulty in obtaining accurate i_0 at higher T. The vanadium-ion concentration is 0.2 M dissolved in 1 M H_2SO_4 , except for GC (0.5 M H_2SO_4). The kinetics of V^{2^+}/V^{3^+} reaction on GC is almost unchanged with changing acid concentration from 0.5 to 1.0 M H_2SO_4 (Figure S19). All kinetic parameters of GC and EPPG are reproduced from our prior works. Refer to text for references.

potentials on W (Figure S8). Analyzing only the oxidation region ensures the contribution of HER on the estimated i_0 is minimal.^{33,46} Electrochemical impedance spectroscopy measurements at open-circuit voltage are fitted to a modified Randles circuit (Scheme S1) to estimate exchange current densities from CT resistance method $(i_{0,R_{rt}})$. The variation of i_0 with temperature is fitted to the Arrhenius equation to estimate $E_{\rm a}$ (Figures S10-S12) and apparent frequency factors by the Tafel method. Similarly, the variation of $i_{0,R_{ct}}$ with temperature is used to estimate apparent activation energies $(E_{a,R_{a}})$, and CT apparent frequency factors (Figures S10 and S11). The agreement between the kinetic parameters obtained from the independent Tafel and CT resistance methods (Figures S9-S12 and Table S1) assists in ensuring reproducibility and provides information pertaining to the number of electrons involved in the reaction. More experimental details regarding the rate measurements are in the Supporting Information.

The large effect of the electrode surface on the exchange current density in Figure 1a shows that the V^{2+}/V^{3+} reaction is inner sphere. The i_0 of the V^{2+}/V^{3+} reaction on all five electrodes (Au, Ag, Cu, Bi, and W) measured in this work are compared with i_0 on glassy carbon (GC) and edge plane pyrolytic graphite (EPPG) from our prior works and are shown as a function of state of charge $\left(SoC = \frac{[V^{2+}]}{[V^{2+}] + [V^{3+}]}\right)$ in Figure 1a. We measure the SoC by deconvoluting the contributions of

 V^{2+} and V^{3+} using UV-vis spectroscopy. ⁴⁶ All metal electrodes have a higher i_0 than Bi and follow the order W > Cu > Ag > Au > Bi at 50% SoC. The 3 orders of magnitude variation in i_0 between the most active (W) and least active (GC) electrode in Figure 1a is much larger than the factor of 3-8 times observed for different electrodes for outer-sphere reactions of transition-metal ions, 3^{4-37} suggesting that the V^{2+}/V^{3+} is an inner-sphere reaction. Additionally, the 3 orders of magnitude rate enhancement on metals compared to carbon confirm that the catalyzing effect observed previously for metals deposited on carbon supports for the V²⁺/V³⁺ reaction is largely due to the metals themselves and not due to changes in the properties of carbon supports because of metal deposition. We discuss controls related to the electrode surface in the Supporting Information (Figures S13–S15). By comparing i_0 and $i_{0,R_{ct}}$ on different electrodes except W, we show that the ratedetermining step (RDS) of V²⁺/V³⁺ reaction involves one electron transfer on all metals (Table S2), similar to GC and EPPG in $\rm H_2SO_4$. 32,46

The dependence of V^{2+}/V^{3+} kinetics on SoC for all electrodes also implies that V^{2+}/V^{3+} is an inner-sphere reaction with electron transfer as the RDS. W, Cu, Ag, and Bi show a maximum in i_0 between 30 and 80% SoC similar to EPPG, whereas i_0 on Au decreases with decreasing SoC similar to GC as shown in Figure 1a. An outer-sphere reaction would not have a decreasing i_0 with SoC, as we have previously discussed.³³ Hence, we consider a simplified inner-sphere CT

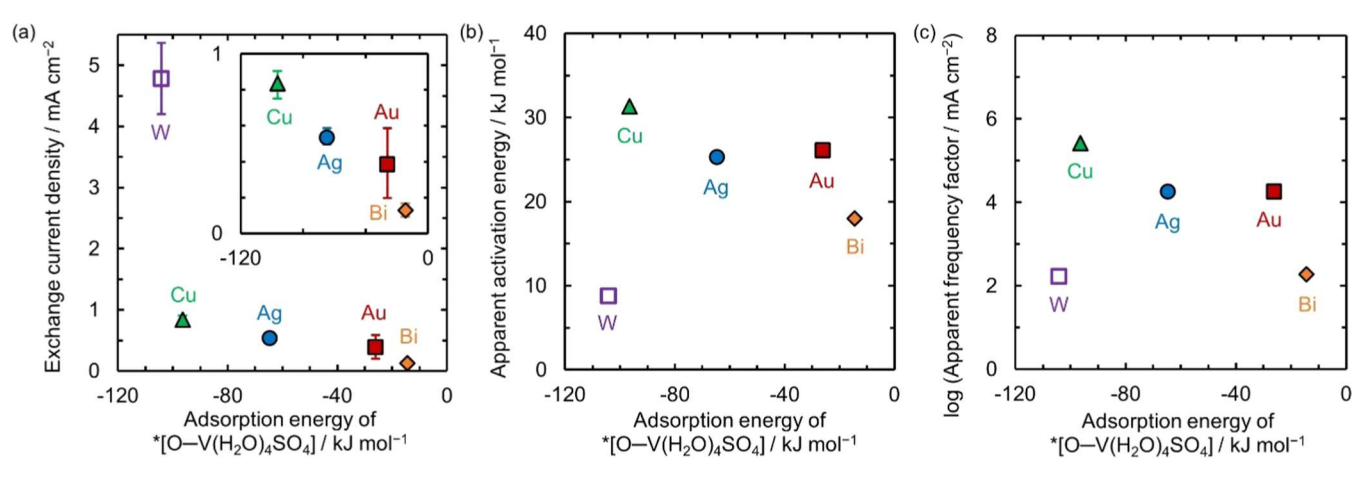


Figure 2. V^{2+}/V^{3+} kinetic parameters on metals compared to adsorption energies of intermediates on various metal electrodes. (a) Exchange current density at room temperature (T = 23.3 °C), (b) apparent activation energy, and (c) logarithmic of apparent frequency factor at 50% state of charge in H_2SO_4 as a function of calculated adsorption energies of * $[O-V(H_2O)_4SO_4]$ on Au, Ag, Cu, Bi, and W electrodes for V^{2+}/V^{3+} reaction. The inset in (a) shows zoomed version of the plot excluding W.

reaction mechanism with three elementary steps involving adsorption, electron transfer, and desorption, consistent with the reaction mechanism that explains the V^{2+}/V^{3+} kinetic behavior with SoC in different electrolytes. The rate law for inner-sphere CT reaction with electron transfer step as the RDS (eq S24) captures the i_0 behavior with SoC on all electrodes. On the contrary, rate laws assuming either the adsorption or desorption of the vanadium intermediate as the RDS are unable to capture the i_0 behavior on all electrodes (Tables S3 and S4). Although we consider a simplified reaction mechanism here, we recognize that the inner-sphere CT mechanism might be more complex, such as involving ion transfer or electron transfer coupled with adsorption or desorption.

The Tafel slopes on all metal and carbon electrodes in Figure 1b indicate that the V^{2+}/V^{3+} reaction is asymmetric with electron transfer as the RDS. For a reaction involving one electron transfer in RDS and completely symmetric (transfer coefficient, $\alpha_{\rm ox}$ = $\alpha_{\rm red}$ = 0.5), the Tafel slope is ~117 mV/ decade at room temperature (T = 23.3 °C) and independent of SoC. 48 The Tafel slopes are between 130 and 170 mV/decade on Au, Bi, EPPG, and GC and between 200 and 250 mV/ decade on Cu and Ag. On the contrary, Tafel slopes are close to 60 mV/decade on W. The use of V^{2+}/V^{3+} oxidation region to estimate i₀ and Tafel slopes greater than 117 mV/decade on all electrodes except W indicate that the V2+/V3+ reaction is asymmetric with α_{ox} lower than 0.5. The relatively constant Tafel slopes with varying SoC confirm that the electron transfer is the RDS on all electrodes as shown in the Supporting Information. However, the reaction mechanisms with adsorption, electron transfer, or desorption steps as RDS do not explain the very low Tafel slopes on W, indicating the possibility of a more complex reaction mechanism on W. Asymmetric transfer coefficients have been previously reported for several redox reactions including $Fe^{2^{+}}/Fe^{3^{+}}$, $Co^{3^{+}}/Co^{2^{+}}$, and $Cr^{2^{+}}/Cr^{3^{+}}$ on metal electrodes. $^{38,39,49-52}$

The variation of E_a and apparent frequency factor with SoC also indicates that the electron transfer step is the RDS for V^{2+}/V^{3+} reaction on all electrodes except W and EPPG. On all electrodes except W and EPPG, the E_a and apparent frequency factor continuously increase with decreasing SoC as shown in Figure 1c,d, respectively. The increasing E_a and apparent

frequency factor with decreasing SoC agree with predicted trends for a reaction mechanism with electron transfer step as the RDS (Figure S17). W and EPPG show a minimum in both E_a and apparent frequency factor with SoC as shown in Figure 1c,1d. The reaction mechanisms with adsorption, desorption, or electron transfer step as the RDS (Figures S16–S18) do not predict a minimum in E_a and apparent frequency factor with SoC, indicating the reaction mechanism on W and EPPG is possibly different than the other tested electrodes. The rate laws showing the trends in kinetic parameters with SoC are summarized in Table S4 and available in the Supporting Information.

To summarize, the experimental V^{2+}/V^{3+} kinetics shown in Figure 1 points to V^{2+}/V^{3+} being an inner-sphere reaction on metals, with the electron transfer between the adsorbed vanadium intermediate and the surface serving as the RDS. Our previous work on carbon electrodes in different electrolytes indicated that the bridging ligand influenced the adsorption energy of the formed vanadium intermediate (*[X-V^{3+}]) and controlled the rate of the V^{2+}/V^{3+} reaction. ^{32,33} We propose that the electrode will influence the adsorption energy of the vanadium intermediate on different metal electrodes.

We hypothesize that a vanadium species adsorbed through an *O bridge is the CT intermediate in H₂SO₄, and the energy of this intermediate affects the i_0 for metals. We demonstrated previously that V2+ adsorbs as *[OH-V(H2O)5]+ bridged intermediate in H₂SO₄.^{33,46} Alternatively, the bridging ligand may come from *OH on the surface (Table S5). To explore this possibility, we determine the equilibrium coverage of *OH on different metals by calculating the adsorption energy of *OH at the V^{2+}/V^{3+} redox potential as a function of coverage using density functional theory (DFT) (Table S5). The equilibrium coverage is the coverage at which adsorption is most thermodynamically favored. All coverage calculations are performed using the Vienna Ab initio Simulation Package (VASP).⁵³ Additional details are provided in the Supporting Information. Among all of the metals tested, *OH has a favorable equilibrium coverage only on Cu and W. Therefore, the bridging ligand cannot come from *OH on the surface of Au, Ag, and Bi, although this is plausible on Cu and W. Once adsorbed, the $*[OH-V(H_2O)_5]^+$ intermediate undergoes

electron transfer and a ligand exchange to form *[OH– $V(H_2O)_4SO_4$]. We expect ligand exchange to occur immediately after the electron transfer step in the RDS because the ligand exchange of V^{3+} with $SO_4^{\ 2-}$ is thermodynamically favored. We consider the *[OH– $V(H_2O)_4SO_4$] intermediate kinetically relevant in comparison to *[OH– $V(H_2O)_5$]+ based on our prior work. We observe in our DFT-based metadynamics calculations that *[O– $V(H_2O)_4SO_4$] is more favorable to form on metals compared to *[OH– $V(H_2O)_4SO_4$]. Because the energies of reaction intermediates are difficult to extract experimentally, we compute the adsorption free energy of the *[O– $V(H_2O)_4SO_4$] in the next section and determine if there is a correlation between the adsorption energy and the CT kinetics.

2.2. Adsorption Energy of the Vanadium Intermediate as a Descriptor of V^{2+}/V^{3+} Reaction Kinetics and Correlation with the d-Band Center of the Electrode. We evaluated the adsorption free energy of the *[O- $V(H_2O)_4SO_4$] intermediate using DFT-based metadynamics simulations in VASP. Metadynamics is an enhanced sampling technique involving the use of artificial bias potentials to fill free energy minima as a function of a collective variable. S4,55 Here, we use the *z*-coordinate of the vanadium ion as the collective variable and use the sum of the bias potentials to estimate the free energy of adsorption. The simulation cell used for metadynamics calculations (Figure S20), free energy profiles of the adsorbed vanadium intermediate on metals (Figure S21), and more details of evaluating adsorption free energies are given in the Supporting Information.

The computed adsorption free energies of *[O-V- $(H_2O)_4SO_4$] rationalize the kinetic trends of the V^{2+}/V^{3+} reaction on metal electrodes. We show the i_0 , E_a , and apparent frequency factor at 50% SoC vs the adsorption free energy of * $[O-V(H_2O)_4SO_4]$ in Figure 2. The i_0 in Figure 2a increases with stronger adsorption of the intermediate following the order W > Cu > Ag > Au > Bi (Table S6) confirming our hypothesis that changing the metal electrode alters the reaction energy profile by changing the adsorption energy. The inset in Figure 2a shows that a linear trend holds even after removing the most active electrocatalyst W from our analysis. We expect that as the adsorption energy decreases, both the intermediate coverage and the E_a would increase. The higher intermediate coverage would lead to a larger apparent frequency factor. The stronger adsorption would make the desorption more difficult, increasing E_a . All metals except W obey these trends, as shown by the increasing E_a and apparent frequency factor with decreasing adsorption energy in Figure 2b,c, respectively. However, W has different Tafel slopes and a different dependence of Ea and apparent frequency factor on SoC compared to other metals and is most active with the lowest E_a . The different dependence on SoC and low E_a on W for low adsorption energy indicates that the V2+/V3+ reaction occurs through a different reaction mechanism on W. A more complex reaction mechanism involving the formation of several intermediates, multiple rate-controlling steps like ion transfer or electron transfer coupled with adsorption/desorption can potentially explain the differences in Tafel slopes, V^{2+}/V^{3+} kinetic trends with SoC, and low E_a and apparent frequency factor for low adsorption energy on W. Regardless, the i_0 increases with decreasing adsorption energy, indicating that the electrodes that bind *[O-V(H₂O)₄SO₄] more strongly are more active.

The adsorption free energy of $*[O-V(H_2O)_4SO_4]$ correlates with the d-band center as shown in Figure 3. We

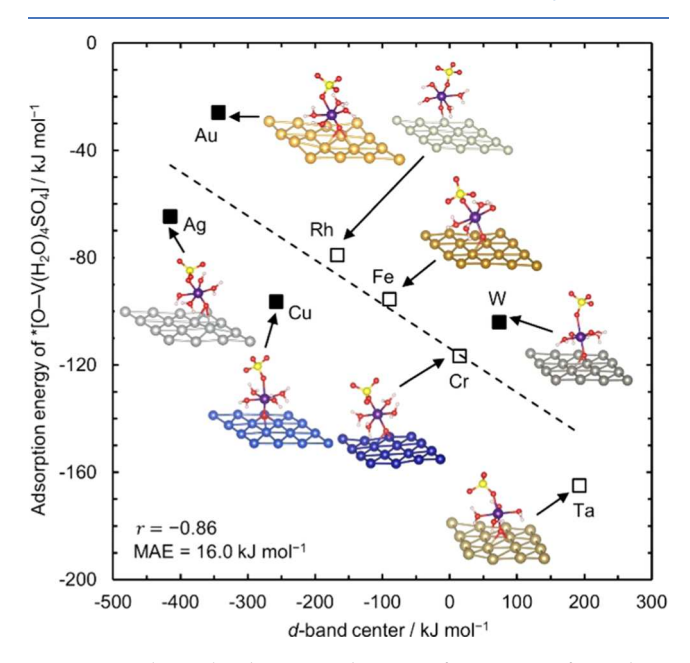


Figure 3. Relationship between adsorption free energy of vanadium intermediate and d-band center of the electrode. Adsorption free energy of $*[O-V(H_2O)_4SO_4]$ shown against the d-band center. The solid squares are the metals that we experimentally tested for kinetics and hollow squares are additional metals chosen to span a wider range of d-band centers of metals. Linear trendline along with the geometries of adsorbed intermediates on each metal electrode is indicated. r is the Pearson correlation coefficient, and MAE is the mean absolute error. The d-band center for metals used in the analysis is available in Table S9. Atom color legend: red = O, light yellow = S, purple = V, white = H, yellow = Au, light gray = Rh, silver = Ag, dark gray = W, blue = Cu, dark blue = Cr, ginger = Fe, and brown = Ta. Adsorption free energies were evaluated at 300 K using metadynamics.

observe that the adsorption energy of the $*[O-V(H_2O)_4SO_4]$ intermediate correlates strongly (Pearson correlation coefficient, r = -0.86) with the d-band center of the electrode. The low mean absolute error (MAE = 16.0 kJ/mol) also indicates the d-band center can be used as an alternative to adsorption energy to correlate with the V^{2+}/V^{3+} redox kinetics. We compute adsorption energies on additional metals including Fe, Cr, Rh, and Ta that cannot be tested experimentally due to their instability under reaction conditions or side reactions in addition to the ones we test experimentally (Au, Ag, Bi, Cu, and W) to cover the entire range of the d-band center of metals and test the broad applicability of the correlation. The correlation between the adsorption energy of the vanadium intermediate and d-band center exists because the d-band center controls the strength of the electrode-oxygen bond and thus is indicative of the adsorption strength of the intermediate. Resultantly, we hypothesize that the d-band center should correlate with the V^{2+}/V^{3+} kinetics on various metal electrodes, which we explore in the next section. We observe a similar linear correlation between gas-phase adsorption free energies of the vanadium intermediate and dband center of the electrode (Figure S22 and Table S7), indicating that solvent effects do not change the identified qualitative trends, although the absolute numbers are different. Gas-phase adsorption free energies are based on the ideal gas

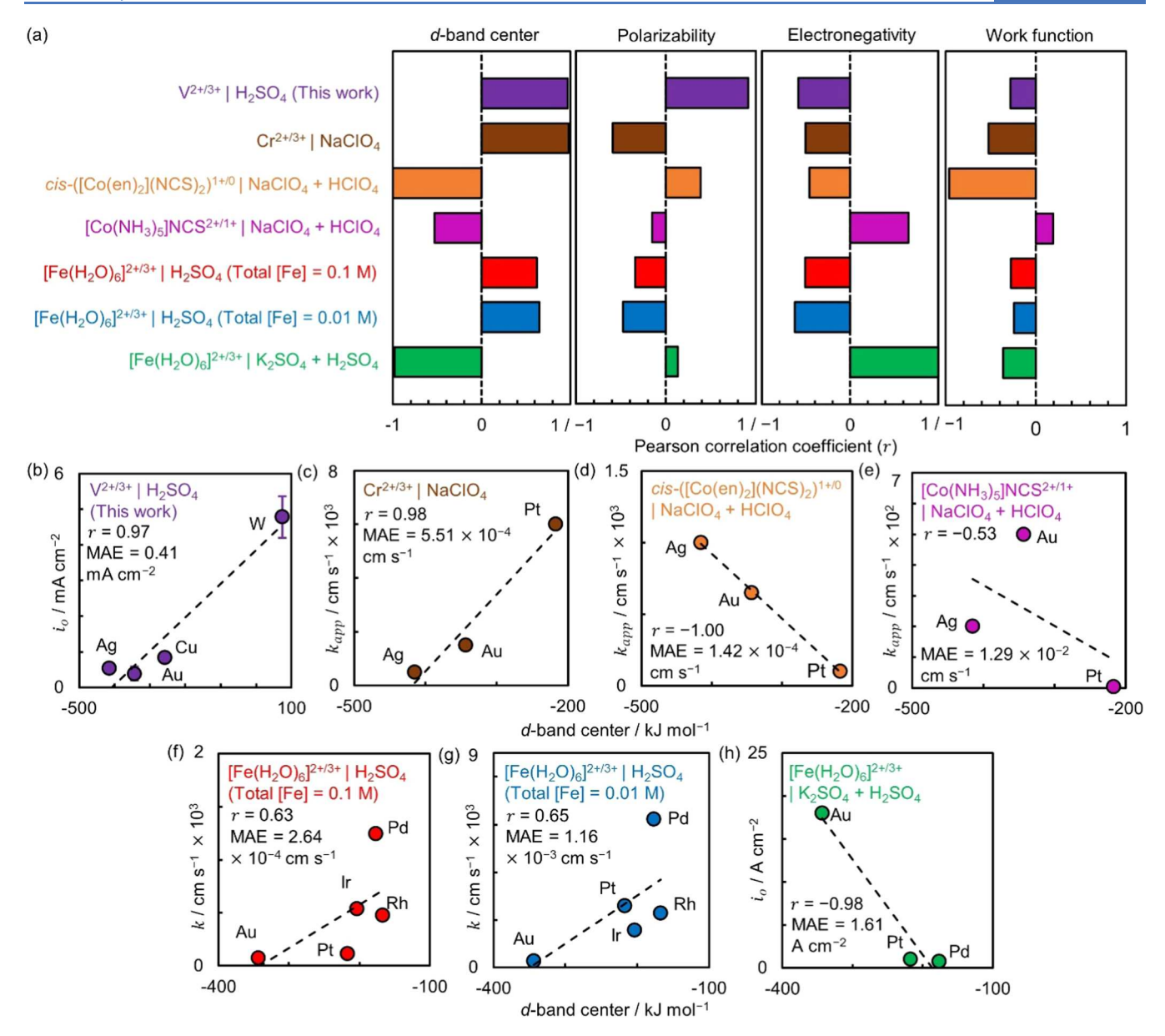


Figure 4. Correlation between kinetics of inner-sphere charge transfer reactions of transition-metal ions and electrode properties. (a) Pearson correlation coefficient (r) for linear correlations of exchange current densities (i_0) or standard (k) or apparent (k_{app}) rate constants for various inner-sphere redox couple | electrolyte combinations vs d-band center of the electrode, electrode polarizability, electronegativity, and work function. (b-h) i_0 or k or k_{app} for various inner-sphere redox couple | electrolyte combinations linearly correlating with the d-band center of the electrode with r and mean absolute error (MAE) shown in the inset. The raw kinetic data for all analyzed redox couples extracted from the literature and metal electrode properties used to determine the correlations are available in Tables S8 and S9, respectively.

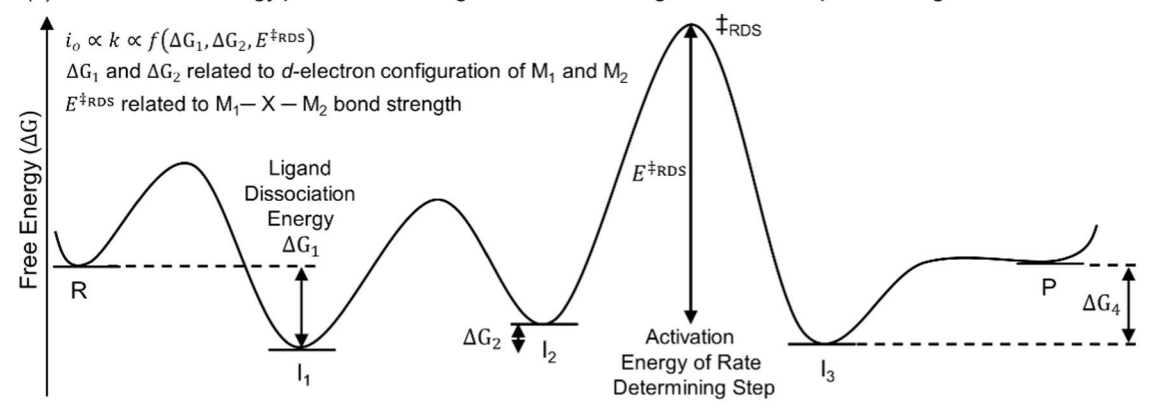
harmonic oscillator model, as explained in the Supporting Information.

2.3. d-Band Center as a Descriptor for Heterogeneous Inner-Sphere Charge Transfer of V-, Fe-, Co-, and Cr-Metal Ions. To explore if the d-band center or other electrode properties explain kinetic trends of V^{2+}/V^{3+} and het-CT of various other transition-metal ions, we extract kinetic data for four het-CT reactions from the literature to add to our V^{2+}/V^{3+} work here. To avoid lab-to-lab variations in the reported k or i_0 for a redox couple on the same electrode we only compare kinetic data from the same laboratory measured using the same methods. Additionally, to control for the effect of the anion on rate constants, we only compare kinetic data in the same electrolyte. To ensure sufficient points to draw a correlation, we only select CT reactions where a

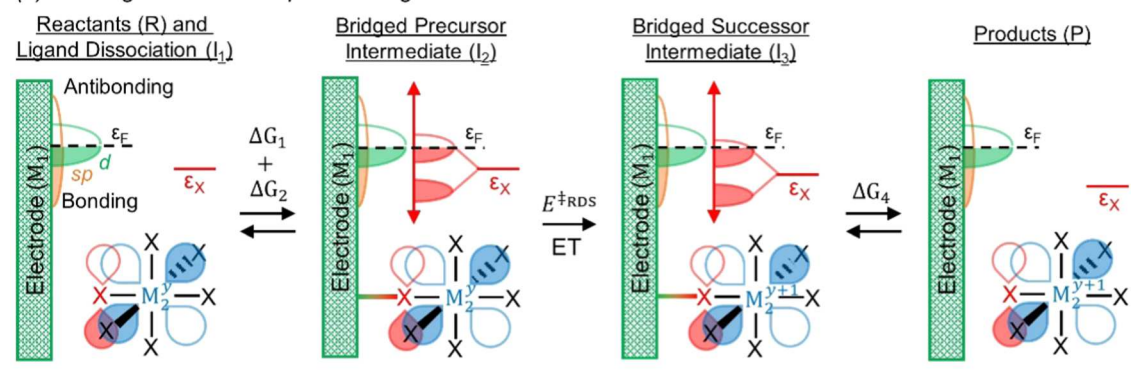
minimum of three metals are used as electrodes. These criteria result in six sets of data to add to ours for V^{2+}/V^{3+} in H_2SO_4 . Three of those sets of data are for the same redox couple (Fe^{2+}/Fe^{3+}) but done in different laboratories with varying total Fe concentration and supporting electrolyte. The six data sets include the kinetic rate constants of $[Fe(H_2O)_6]^{2+/3+}$ in H_2SO_4 (with total [Fe] = 0.1 and 0.01 M) and mixture of K_2SO_4 and H_2SO_4 (Fe^{2+}/Fe^{3+}) , 40,41 $[Co(NH_3)_5]NCS^{2+/1+}$ and cis- $([Co(en)_2](NCS)_2)^{1+/0}$ in mixture of NaClO₄ and HClO₄ (Co^{3+}/Co^{2+}) , 39 and Cr^{2+}/Cr^{3+} in NaClO₄ (Table~S8). 38 The anions present in the electrolyte or part of the coordination sphere, e.g., OH^- , NCS^- , $SO_4^{\ 2-}$, act as bridging ligands to form adsorbed metal-ion intermediate for these redox reactions undergoing het-CT similar to V^{2+}/V^{3+} . 31

Scheme 1. Inner-Sphere Charge Transfer Reactions of Transition-Metal Ions at Electrode and in Solution

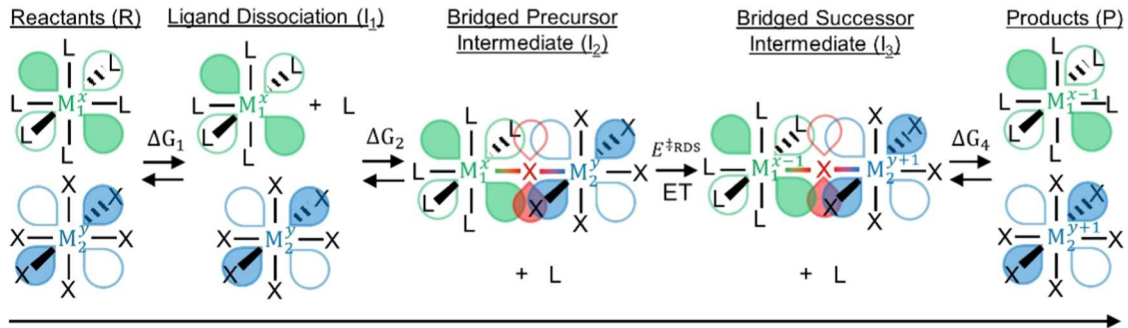
(a) Reaction free energy profile for heterogeneous and homogeneous inner-sphere charge transfer



(b) Heterogeneous inner-sphere charge transfer mechanism



(c) Homogeneous inner-sphere charge transfer mechanism



Reaction Coordinate

"(a) Free energy diagram showing typical steps involved in inner-sphere CT of transition-metal ions. Reactant (R), intermediates (I_1 , I_2 , and I_3), and products (P) are denoted. The exchange current density and rate constant are a function of the reaction energetics. ΔG_i is the free energy change of step i, and $E^{\ddagger_{RDS}}$ is the activation energy of the rate-determining step. Corresponding reaction steps for (b) heterogeneous and (c) homogeneous inner-sphere CT involving transition metals M_1 and M_2 . Here, x is the oxidation state of M_1 in homogeneous CT and y is the oxidation state of M_2 in homogeneous and heterogeneous CT. L and X are neutral ligands. The density of states of electrode M_1 and d-orbitals of metal ion M_2 for het-CT and d-orbitals of metal ions M_1 and M_2 is shown for hom-CT. The p-orbitals of bridging ligand X are also shown. ET is electron transfer, ε_X is the electronic energy of the p-orbital of ligand X, and ε_F is the electrode Fermi-level energy with respect to the vacuum.

The kinetics of all five het-CT reactions linearly correlate best with the d-band center of the electrode in comparison to other electrode properties proposed to influence het-CT kinetics in the literature. The data in Figure 4a shows that r for kinetics is largest for the d-band center compared to electrode polarizability, electronegativity, and work function. The kinetics might also correlate to several combinations of electrode properties, especially for redox couples with moderate absolute values of r (0.5–0.7); however, in this work, we choose a single electrode property to follow the principle of Occam's razor. Even though the electrode

electronegativity for $[Fe(H_2O)_6]^{2^{+/3+}}$, electrode work function for cis- $([Co(en)_2](NCS)_2)^{1+/0}$, and electrode polarizability for V^{2^+}/V^{3^+} also lead to good linear correlations (|r| > 0.5), d-band center is the only electrode property that shows good correlations for all analyzed CT reactions as depicted in Figure 4a. We observe that the kinetics of het-CT reactions correlate best with the d-band center regardless of the way the kinetics is mathematically represented (Figure S23). Although our analysis is limited to only five inner-sphere CT reactions due to limited availability of rate constants, the high r value for the d-band center of the electrode for all CT reactions suggests

that the d-band center can be used as a descriptor for understanding and capturing the effect of electrode on the het-CT reactions. The availability of more kinetic data for innersphere CT reactions on multiple metal electrodes in the same electrolyte will help in further confirming this analysis.

We propose the positive or negative sign of the correlation between kinetics and d-band center depends on whether increasing the adsorption strength of the metal-ion intermediate increases or decreases the rate. The kinetics linearly correlate with the d-band center for all five het-CT reactions. The kinetics of V^{2+}/V^{3+} in H_2SO_4 (Figure 4b), Cr^{2+}/Cr^{3+} (Figure 4c), and $[Fe(H_2O)_6]^{2+/3+}$ in H_2SO_4 (Figure 4f,g) correlate positively with the d-band center. On the other hand, the kinetics of cis-([Co(en)₂](NCS)₂)^{1+/0} (Figure 4d), [Co- $(NH_3)_5 NCS^{2+/1+}$ (Figure 4e), and $[Fe(H_2O)_6]^{2+/3+}$ in a mixture of K₂SO₄ and H₂SO₄ (Figure 4h) correlate negatively with the d-band center. The r of correlations vs d-band center is improved if the kinetics is considered in the logarithmic scale; however, the sign of the correlation for all redox couples is unchanged (Figure S23). For V2+/V3+ and the others with positive correlations, a higher d-band center increases the adsorption strength of the intermediates, increasing the rate. If the intermediate adsorbs too strongly, the kinetics will decrease with higher d-band center leading to a negative correlation because the electrode will adsorb the intermediate even more strongly, and desorption becomes more difficult. Resultantly, there is an optimum value for intermediate adsorption strength or d-band center of the electrode that would maximize the CT kinetics based on Sabatier's principle. 58 Figure 4e shows the kinetics of [Co(NH₃)₅]NCS^{2+/1+} are faster on Au compared to Ag and Pt indicating that possibly the d-band center of Au allows the intermediate to adsorb with optimum adsorption strength, maximizing the kinetics. However, kinetics of [Co(NH₃)₅]NCS^{2+/1+} on more metal electrodes is needed to confirm this. The positive d-band center correlation of $[Fe(H_2O)_6]^{2+/3+}$ kinetics in H_2SO_4 vs the negative correlation of kinetics in K2SO4 and H2SO4 may arise because of the presence of potassium cations influencing the double-layer structure and the d-band center of the metal electrode or due to the differences in complexation of Fe²⁺ and Fe³⁺ species in these electrolytes, which affect the bridge involved in the formation of the adsorbed metal-ion intermediate. Regardless of the changing sign of correlations in Figure 4b-h, the MAE for correlations of kinetics vs d-band center is at least an order of magnitude smaller in comparison to the kinetics on the most active metal for all five het-CT reactions, indicating the correlations capture the kinetic trends on metals quantitatively.

Compared to the d-band center, the smaller r value for electrode properties like polarizability, electronegativity, and work function is expected because none of those other electrode properties govern the adsorption strength of the bridged intermediate. The identification of the d-band center as a descriptor will enable the rational design of bimetallic alloys or core—shell catalysts with a desired d-band center to improve redox kinetics for het-CT reactions.

3. DISCUSSION

It is critical to understand the reaction energetics and mechanism to rationalize the correlation of the d-band center with the kinetics of heterogeneous inner-sphere CT reactions. Here we discuss how the kinetic parameters, that is, i_0 or k, E_a , and apparent frequency factor, depend on a general reaction free energy diagram for forming an oxidized product P from a

reduced reactant R, as depicted in Scheme 1a. Inner-sphere CT of transition-metal ions involves multiple elementary steps with the formation of intermediates in series. Here we assume three intermediates form: I1, I2, and I3. The energies of the intermediates and of the transition states of these elementary steps dictate the overall rate of charge transfer (Scheme 1a). For the case where electron transfer to form I₃ is the RDS, the apparent frequency factor is related to the concentration of the intermediates (I₁ and I₂) formed in steps before the RDS and depends on the free energies of forming I_1 (ΔG_1) and I_2 (ΔG_2) . The E_a is related to the difference in the transition states (\ddagger_{RDS}) energy and the energy of I_2 , denoted by $E^{\ddagger_{RDS}}$. Therefore, with ΔG_1 , ΔG_2 , and $E^{\ddagger_{RDS}}$, one can in principle predict the kinetics of charge transfer for inner-sphere CT. The rate law's dependence on $\bar{\Delta}G_1$, ΔG_2 , and $E^{\ddagger_{\text{RDS}}}$ for inner-sphere CT is shown in the Supporting Information. If the electron transfer step is not the RDS or multiple reaction steps are ratecontrolling, the kinetics of CT will depend on the free energies of relevant intermediates and transition state energies. For heterogeneous inner-sphere CT (het-CT), the free energy of the final step from I_3 to P (ΔG_4) is the energy of intermediate I_3 and is related to $E^{\ddagger_{RDS}}$ by adsorbate scaling relationships.⁵⁸ The intermediate I₃ is an adsorbed, oxidized metal ion for het-CT (Scheme 1b), which for V^{2+}/V^{3+} is *[O-V(H₂O)₄SO₄]. We show above that i_0 , E_a , and apparent frequency factors scale with the computationally predicted adsorption energies (ΔG_4) of *[O-V(H₂O)₄SO₄] on metal electrodes in Figure 2.

The coupling of the energy levels between the metal ion and the electrode, the d-electron configuration of the metal ion, and the ligand field strength affect ΔG_1 , ΔG_2 , and $E^{\ddagger_{RDS}}$ for het-CT. In het-CT, one of the redox species is an electrode (M_1) , so in Scheme 1b, we depict the density of states and Fermilevel $(\varepsilon_{\rm F})$ for M₁. We also show the electronic energy $(\varepsilon_{\rm X})$ of the p-orbital of the ligand X in metal-ion complex $M_2^y X_6$. $M_2^y X_6$ adsorbs on M_1 to form I_2 . ΔG_1 ($M_2^{\gamma}X_6$ ligand dissociation) and ΔG_2 ($M_2^y X_6$ adsorption to M_1) depend on the d-electron configuration of M2 and the ligand field strength of X. Additionally, ΔG_2 also depends on the electronic structure of M₁. I₂ undergoes electron transfer in the RDS through transition state \ddagger_{RDS} to form $M_1 - X - M_2^{y+1}X_5$ (that is, I_3 or *[X - $M_2^{\gamma+1}$]). Here, we consider the bridging ligand X comes from metal ion M2's coordination sphere, however, X present on electrode M₁ initially could also participate in forming the intermediate. I₃ desorbs to form the product P. The adsorption energy of the metal ion on the electrode through the bridging ligand (*[X - M_2^{y+1}]) depends on the electronic structure of the electrode and controls $E^{\ddagger_{RDS}}$. From a molecular perspective, for a fixed ligand X and metal ion M2, the adsorption strength of X on electrode M₁ is dictated by the occupancy of the antibonding states of X, which depends on the position of antibonding states relative to $\varepsilon_{\rm F}$. The positions of antibonding states of atomic adsorbates such as H, N, O, and S and molecular adsorbates such as CO, NO, and C2H4 are described well by the d-band center of the electrode (i.e., average energy of the d-electrons with respect to $\varepsilon_{\rm F}$). S9-62 The occupancy of antibonding states of X is higher with a lower d-band center, which leads to weaker adsorption of X. The weaker adsorption of X leads to weaker adsorption of the *[X - M_2^{y+1}] intermediate for fixed X and M2 and vice versa. This d-band model has successfully rationalized kinetic trends of several inner-sphere reactions in heterogeneous catalysis that involve the formation of an adsorbed intermediate such as HER^{60,61} and the oxygen reduction reaction.⁶² Since we observe similar

trends between the d-band center and adsorption energies for metal ion adsorbate, i.e., $*[O-V(H_2O)_4SO_4]$ in Figure 3, the d-band center captures the coupling of energy levels between the metal ion and electrode and rationalizes the effect of the electrode on the kinetics of het-CT of transition-metal ions in Figure 4.

The influence of the d-band center on the kinetics of het-CT is analogous to the influence of d-electron configuration for homogeneous inner-sphere CT (hom-CT). In hom-CT (Scheme 1c), the reactants undergo CT as two metal ions in solution, $M_1^x L_6$ and $M_2^y X_6$. $M_1^x L_6$ first loses ligand L to form I_1 , with energy ΔG_1 .³¹ Next, $M_1^x L_5$ and $M_2^y X_6$ form a bridged precursor intermediate I_2 ($L_5M_1^x - X - M_2^yX_5$) with free energy of reaction ΔG_2 . ³¹ I₂ subsequently undergoes electron transfer with activation energy $E^{\ddagger_{RDS}}$ to form a bridged successor intermediate I₃, which proceeds to form the products P. The free energy to form P, i.e., ΔG_4 accounts for the changes in the structure of I₃ and ligand association energies of products $M_1^{x-1}L_6$ and $M_2^{y+1}X_6$. The d-electron configuration of metal ions M₁ and M₂ and the ligand field strength of ligand X govern the d-orbitals involved in forming I_1 and I_2 and control ΔG_1 and ΔG_2 . The symmetry of the d-orbitals of the metal ions available for overlapping with the p-orbitals of the bridging ligand controls the M_1 –X– M_2 bond strength, and hence $E^{\ddagger_{RDS}}$ and E_a .³¹ The properties that control ΔG_1 , ΔG_2 , and $E^{\ddagger_{RDS}}$ and hence the rate for hom-CT (Scheme 1c) include the d-electron configuration of the transition-metal-ion redox couples and the ligand field strength. The d-electron configuration controlling the bridged intermediate bond strength in hom-CT is similar to the d-band center controlling the intermediate adsorption strength for het-CT, indicating analogous reaction mechanisms for homogeneous and heterogeneous inner-sphere CT.

4. CONCLUSIONS

Intrinsic kinetic measurements for the V²⁺/V³⁺ reaction on five metal electrodes demonstrate that W is the most active electrocatalyst for the V^{2+}/V^{3+} reaction reported thus far. The large variation in exchange current density with the electrode explains the electrocatalytic effect of metals in redox flow batteries and confirms that the V2+/V3+ is an inner-sphere charge transfer reaction, involving an adsorbed intermediate. The V²⁺/V³⁺ kinetics correlates with the adsorption strength of the intermediate, rationalizing the effect of the electrode. We identify that the d-band center of the electrode controls the adsorption strength of the metal ion intermediate and hence correlates with kinetics of several heterogeneous inner-sphere CT reactions. The linear correlation of the redox kinetics with the d-band center we report here for reactions involving transition-metal-ion adsorbates is similar to correlations for many heterogeneous catalytic reactions involving atomic and molecular adsorbates. The observation that the d-band center controls the heterogeneous inner-sphere charge transfer rate is also analogous to the d-electron configurations of transitionmetal ions controlling rates in homogeneous inner-sphere charge transfer. The d-band center of a metal electrode can be tuned by alloying with different metals at various compositions, nanostructuring (e.g., changing the fraction of exposed surface facets), or introducing lattice strain, opening an avenue to design electrodes for heterogeneous inner-sphere charge transfer reactions of transition-metal ions.

ASSOCIATED CONTENT

Data Availability Statement

Computational data for this paper, including VASP input files, output files, geometries, and scripts, are available at the NOMAD Repository at https://dx.doi.org/10.17172/NOMAD/2022.12.28-1.

Solution Supporting Information

The Supporting Information is available free of charge at https://pubs.acs.org/doi/10.1021/acscatal.2c05694.

Preparation of metal electrodes; cleaning and measurement of electrochemically active surface area of metal electrodes; V^{2+}/V^{3+} rate measurements on metal electrodes; hydroxyl coverage on various metal electrodes; V^{2+}/V^{3+} adsorption energies on metal electrodes from metadynamics; DFT-calculated gas-phase adsorption energies of V^{2+}/V^{3+} on metal electrodes; rate constants of transition-metal-ion redox couples on metal electrodes; and proposed rate law for homogeneous innersphere charge transfer (PDF)

AUTHOR INFORMATION

Corresponding Author

Nirala Singh — Department of Chemical Engineering, University of Michigan, Ann Arbor, Michigan 48109-2136, United States; Catalysis Science and Technology Institute, University of Michigan, Ann Arbor, Michigan 48109-2136, United States; orcid.org/0000-0003-0389-3927; Email: snirala@umich.edu

Authors

Harsh Agarwal – Department of Chemical Engineering, University of Michigan, Ann Arbor, Michigan 48109-2136, United States; Catalysis Science and Technology Institute, University of Michigan, Ann Arbor, Michigan 48109-2136, United States; orcid.org/0000-0002-5237-4819

Jacob Florian — Department of Chemical Engineering, University of Michigan, Ann Arbor, Michigan 48109-2136, United States; Catalysis Science and Technology Institute, University of Michigan, Ann Arbor, Michigan 48109-2136, United States; orcid.org/0000-0003-1895-8463

Daniel Pert – Department of Chemical Engineering, University of Michigan, Ann Arbor, Michigan 48109-2136, United States; Catalysis Science and Technology Institute, University of Michigan, Ann Arbor, Michigan 48109-2136, United States

Bryan R. Goldsmith — Department of Chemical Engineering, University of Michigan, Ann Arbor, Michigan 48109-2136, United States; Catalysis Science and Technology Institute, University of Michigan, Ann Arbor, Michigan 48109-2136, United States; orcid.org/0000-0003-1264-8018

Complete contact information is available at: https://pubs.acs.org/10.1021/acscatal.2c05694

Author Contributions

N.S. and H.A. conceived the project. H.A. carried out all experiments and data analysis under the guidance of N.S. J.F. and D.P. performed all of the molecular simulations and DFT modeling under the guidance of B.R.G. All authors were involved in analysis and writing the manuscript.

Funding

This research was funded by University of Michigan Office of Research Grant (UMOR-29814), start-up funds of N.S., and

seed funding from Lurie Nanofabrication Facility at University of Michigan. H.A. acknowledges support from Rackham Predoctoral Fellowship by University of Michigan. N.S. acknowledges support from the National Science Foundation (Grant No. 1919444). The authors acknowledge the University of Michigan College of Engineering for financial support and the Michigan Center for Materials Characterization for use of the instruments and staff assistance. This research used the resources of the National Energy Research Scientific Computing Center (NERSC), a U.S. Department of Energy Office of Science User Facility operated under Contract No. DE-AC02-05CH11231 using NERSC award BES-ERCAP0022175.

Notes

The authors declare no competing financial interest.

ACKNOWLEDGMENTS

H.A. thanks Dr. Matthew Oonk and Dr. Pilar Herrera-Fierro for their help in deposition of metals on glassy carbon disks. H.A. thanks Prof. Vincent Pecoraro for insightful discussions regarding inner-sphere reaction mechanisms.

ABBREVIATIONS

 $E_{\rm a}$, apparent activation energy by Tafel method; $E^{\ddagger_{\rm RDS}}$, activation energy of the rate-determining step; CT, charge transfer; EPPG, edge plane pyrolytic graphite; ECSA, electrochemically active surface area; i_0 , exchange current density by Tafel method; $i_{0,R,z}$, exchange current density by charge transfer resistance method; ΔG_p , free energy of step i; GC, glassy carbon; Het-CT, heterogeneous inner-sphere charge transfer; Hom-CT, homogeneous inner-sphere charge transfer; HER, hydrogen evolution reaction; MAE, mean absolute error; r, Pearson correlation coefficient; RDS, rate-determining step; k or $k_{\rm app}$, standard or apparent rate constant; SoC, state of charge; T, temperature; $\ddagger_{\rm RDS}$, transition state of RDS; UPD, underpotential deposition; R, universal gas constant; VASP, Vienna Ab initio Simulation Package; VRFB, vanadium redox flow battery

REFERENCES

- (1) Yruela, I. Transition Metals in Plant Photosynthesis. *Metallomics* **2013**, *5*, 1090.
- (2) Kärkäs, M. D.; Johnston, E. V.; Verho, O.; Akermark, B. Artificial Photosynthesis: From Nanosecond Electron Transfer to Catalytic Water Oxidation. *Acc. Chem. Res.* **2014**, *47*, 100–111.
- (3) Iovan, D. A.; Jia, S.; Chang, C. J. Inorganic Chemistry Approaches to Activity-Based Sensing: From Metal Sensors to Bioorthogonal Metal Chemistry. *Inorg. Chem* **2019**, *58*, 13546–13560.
- (4) Alday, J.; Mazzeo, A.; Suarez, S. Selective Detection of Gasotransmitters Using Fluorescent Probes Based on Transition Metal Complexes. *Inorg. Chim. Acta* **2020**, *510*, No. 119696.
- (5) Paul, B. T.; Manz, D. H.; Torti, F. M.; Torti, S. V. Mitochondria and Iron: Current Questions. Expert Rev. Hematol. 2017, 10, 65-79.
- (6) Bhat, M. A.; Nioradze, N.; Kim, J.; Amemiya, S.; Bard, A. J. In Situ Detection of the Adsorbed Fe(II) Intermediate and the Mechanism of Magnetite Electrodeposition by Scanning Electrochemical Microscopy. *J. Am. Chem. Soc.* **2017**, *139*, 15891–15899.
- (7) Gimenez-Romero, D.; Juan García-Jareño, J.; Agrisuelas, J.; Gabrielli, C.; Perrot, H.; Vicente, F. Formation of a Copper Oxide Layer as a Key Step in the Metallic Copper Deposition Mechanism. *J. Phys. Chem. C* **2008**, *112*, 4275–4280.

- (8) Morales-Guio, C. G.; Liardet, L.; Hu, X. Oxidatively Electrodeposited Thin-Film Transition Metal (Oxy)Hydroxides as Oxygen Evolution Catalysts. J. Am. Chem. Soc. 2016, 138, 8946–8957.
- (9) Newman, R. C.; Sieradzki, K. Metallic Corrosion. *Science* **1994**, 263, 1708–1709.
- (10) Jeon, B.; Sankaranarayanan, S. K. R. S.; van Duin, A. C. T.; Ramanathan, S. Atomistic Insights into Aqueous Corrosion of Copper. *J. Chem. Phys.* **2011**, *134*, No. 234706.
- (11) Frankel, G. S. Pitting Corrosion of Metals: A Review of the Critical Factors. *J. Electrochem. Soc.* **1998**, *145*, 2186–2198.
- (12) Morstein, J.; Höfler, D.; Ueno, K.; Jurss, J. W.; Walvoord, R. R.; Bruemmer, K. J.; Rezgui, S. P.; Brewer, T. F.; Saitoe, M.; Michel, B. W.; Chang, C. J. Ligand-Directed Approach to Activity-Based Sensing: Developing Palladacycle Fluorescent Probes That Enable Endogenous Carbon Monoxide Detection. *J. Am. Chem. Soc.* **2020**, 142, 15917–15930.
- (13) Asl, H. Y.; Manthiram, A. Reining in Dissolved Transition-Metal Ions. *Science* **2020**, *369*, 140–141.
- (14) Robb, B. H.; Farrell, J. M.; Marshak, M. P. Chelated Chromium Electrolyte Enabling High-Voltage Aqueous Flow Batteries. *Joule* **2019**, *3*, 2503–2512.
- (15) Ding, C.; Zhang, H.; Li, X.; Liu, T.; Xing, F. Vanadium Flow Battery for Energy Storage: Prospects and Challenges. *J. Phys. Chem. Lett.* **2013**, *4*, 1281–1294.
- (16) Skyllas-Kazcos, M. Performance Improvements and Cost Considerations of the Vanadium Redox Flow Battery. ECS Trans. **2019**, 89, 29–45.
- (17) Rodby, K. E.; Carney, T. J.; Ashraf Gandomi, Y.; Barton, J. L.; Darling, R. M.; Brushett, F. R. Assessing the Levelized Cost of Vanadium Redox Flow Batteries with Capacity Fade and Rebalancing. *J. Power Sources* **2020**, *460*, No. 227958.
- (18) Liu, Y.; Liang, F.; Zhao, Y.; Yu, L.; Liu, L.; Xi, J. Broad Temperature Adaptability of Vanadium Redox Flow Battery—Part 4: Unraveling Wide Temperature Promotion Mechanism of Bismuth for V^{2+}/V^{3+} Couple. *J. Energy Chem.* **2018**, *27*, 1333—1340.
- (19) Liu, T.; Li, X.; Nie, H.; Xu, C.; Zhang, H. Investigation on the Effect of Catalyst on the Electrochemical Performance of Carbon Felt and Graphite Felt for Vanadium Flow Batteries. *J. Power Sources* **2015**, 286. 73–81.
- (20) Lv, Y.; Zhang, J.; Lv, Z.; Wu, C.; Liu, Y.; Wang, H.; Lu, S.; Xiang, Y. Enhanced Electrochemical Activity of Carbon Felt for V^{2+}/V^{3+} Redox Reaction via Combining KOH-Etched Pretreatment with Uniform Deposition of Bi Nanoparticles. *Electrochim. Acta* **2017**, 253, 78–84.
- (21) Yang, X.; Liu, T.; Xu, C.; Zhang, H.; Li, X.; Zhang, H. The Catalytic Effect of Bismuth for VO₂+/VO²⁺ and V³⁺/V²⁺ Redox Couples in Vanadium Flow Batteries. *J. Energy Chem.* **2017**, *26*, 1–7. (22) Li, B.; Gu, M.; Nie, Z.; Shao, Y.; Luo, Q.; Wei, X.; Li, X.; Xiao,
- J.; Wang, C.; Sprenkle, V.; Wang, W. Bismuth Nanoparticle Decorating Graphite Felt as a High-Performance Electrode for an All-Vanadium Redox Flow Battery. *Nano Lett.* **2013**, *13*, 1330–1335.
- (23) Zhang, Q.; Liu, T.; Zhang, H.; Li, X. Highly Active Ag Nanoparticle Electrocatalysts toward V^{2+}/V^{3+} Redox Reaction. ACS Appl. Energy Mater. **2021**, 4, 3913–3920.
- (24) Shen, J.; Liu, S.; He, Z.; Shi, L. Influence of Antimony Ions in Negative Electrolyte on the Electrochemical Performance of Vanadium Redox Flow Batteries. *Electrochim. Acta* **2015**, *151*, 297–305.
- (25) Kim, M.; Yoo, H.; Lee, G.; Choi, J. Enhanced VRB Electrochemical Performance Using Tungsten as an Electrolyte Additive. *Electrochim. Acta* **2017**, 246, 190–196.
- (26) Wei, L.; Zhao, T. S.; Zeng, L.; Zhou, X. L.; Zeng, Y. K. Copper Nanoparticle-Deposited Graphite Felt Electrodes for All Vanadium Redox Flow Batteries. *Appl. Energy* **2016**, *180*, 386–391.
- (27) Mehboob, S.; Mehmood, A.; Lee, J.-Y.; Shin, H.-J.; Hwang, J.; Abbas, S.; Ha, H. Y. Excellent Electrocatalytic Effects of Tin Through In Situ Electrodeposition on the Performance of All-Vanadium Redox Flow Batteries. *J. Mater. Chem. A* **2017**, *5*, 17388–17400.

- (28) Gahn, R. F.; Hagdorn, N. H.Negative Electrode Catalyst for the Iron Chromium Redox Energy Storage SystemNational Aeronautics and Space Administration: Cleveland, OH; 1985.
- (29) Wu, C. D.; Scherson, D. A.; Calvo, E. J.; Yeager, E. B.; Reid, M. A. A Bismuth-Based Electrocatalyst for the Chromous-Chromic Couple in Acid Electrolytes. *J. Electrochem. Soc.* **1986**, *133*, 2109–2112.
- (30) Arenas, L. F.; Loh, A.; Trudgeon, D. P.; Li, X.; Ponce de León, C.; Walsh, F. C. The Characteristics and Performance of Hybrid Redox Flow Batteries with Zinc Negative Electrodes for Energy Storage. *Renewable Sustainable Energy Rev.* **2018**, *90*, 992–1016.
- (31) Gispert, J. R. Coordination Chemistry, 1st ed.; Wiley-VCH: Weinheim, Germany, 2008; pp 377-402.
- (32) Florian, J.; Agarwal, H.; Singh, N.; Goldsmith, B. R. Why Halides Enhance Heterogeneous Metal Ion Charge Transfer Reactions. *Chem. Sci.* **2021**, *12*, 12704–12710.
- (33) Agarwal, H.; Florian, J.; Goldsmith, B. R.; Singh, N. The Effect of Anion Bridging on Heterogeneous Charge Transfer for V^{2+}/V^{3+} . *Cell Rep. Phys. Sci.* **2021**, *2*, No. 100307.
- (34) Kuhn, A. T.; Randle, T. H. Effect of Oxide Thickness on the Rates of Some Redox Reactions on a Platinum Electrode. *J. Chem. Soc., Faraday Trans.* 1 1985, 81, 403–419.
- (35) Tanimoto, S.; Ichimura, A. Discrimination of Inner and Outer Sphere Electrode Reactions by Cyclic Voltammetry Experiments. *J. Chem. Educ.* **2013**, *90*, 778–781.
- (36) Iwasita, T.; Schmickler, W.; Schultze, J. W. The Influence of the Metal on the Kinetics of Outer Sphere Redox Reactions. *Ber. Bunsenges. Phys. Chem.* **1985**, *89*, 138–142.
- (37) Velmurugan, J.; Sun, P.; Mirkin, M. V. Scanning Electrochemical Microscopy with Gold Nanotips: The Effect of Electrode Material on Electron Transfer Rates. *J. Phys. Chem. C* **2009**, *113*, 459–464.
- (38) Barr, S. W.; Guyer, K. L.; Weaver, M. J. The Dependence of the Kinetics of Some Simple Outer-Sphere Electrode Reactions on the Nature of the Electrode Material. *J. Electroanal. Chem. Interfacial Electrochem.* **1980**, *111*, 41–59.
- (39) Barr, S. W.; Weaver, M. J. Intramolecular Electron Transfer at Metal Surfaces. 1. Relative Energetics of Some Corresponding Outerand Inner-Sphere Pathways Involving Halide and Pseudohalide Bridging Ligands. *Inorg. Chem.* 1984, 23, 1657–1663.
- (40) Bockris, J. O.; Mannan, R. J.; Damjanovic, A. Dependence of Rate of Electrodic Redox Reactions on the Substrate. *J. Chem. Phys.* **1968**, *48*, 1898–1904.
- (41) Bochmann, H. G.; Vielstich, W. On the Reaction Rate of the Fe²⁺/Fe³⁺ Redox Couple in Sulfate Solution. *Electrochim. Acta* **1988**, 33, 805–809.
- (42) Galizzioli, D.; Trasatti, S. Work Function, Electronegativity, and Electrochemical Behaviour of Metals IV. Simple Electron Exchange Reactions. Fe²⁺/Fe³⁺ Redox Couple. *J. Electroanal. Chem. Interfacial Electrochem.* **1973**, 44, 367–388.
- (43) Trasatti, S. Work Function, Electronegativity, and Electrochemical Behaviour of Metals: II. Potentials of Zero Charge and "Electrochemical" Work Functions. *J. Electroanal. Chem. Interfacial Electrochem.* 1971, 33, 351–378.
- (44) Weber, J.; Samec, Z.; Mareček, V. The Effect of Anion Adsorption on the Kinetics of the Fe³⁺/Fe²⁺ Reaction on Pt and Au Electrodes in HClO₄. *J. Electroanal. Chem. Interfacial Electrochem.* 1978, 89, 271–288.
- (45) Jiang, H. R.; Sun, J.; Wei, L.; Wu, M. C.; Shyy, W.; Zhao, T. S. A High Power Density and Long Cycle Life Vanadium Redox Flow Battery. *Energy Storage Mater.* **2020**, *24*, 529–540.
- (46) Agarwal, H.; Florian, J.; R Goldsmith, B.; Singh, N. V²⁺/V³⁺ Redox Kinetics on Glassy Carbon in Acidic Electrolytes for Vanadium Redox Flow Batteries. *ACS Energy Lett.* **2019**, *4*, 2368–2377.
- (47) Park, I. T.; Kim, W.; Kim, E. J.; Bae, S. E.; Kim, J. Y.; Shin, H. C. Electrochemical Reactivity of Chemically Roughened Tungsten Electrodes. *Asian J. Chem.* **2013**, *25*, 7037–7040.

- (48) Bard, A. J.; Faulkner, L. R. Electrochemical Methods: Fundamentals and Applications, 2nd ed.; John Wiley & Sons, Inc.: New York, 2001; pp 331-367.
- (49) Makrides, A. C. Kinetics of Redox Reactions on Passive Electrodes. J. Electrochem. Soc. 1964, 111, 392–400.
- (50) Agarwal, H. P.; Qureshi, S. Faradaic Rectification Studies of the Ferrous-Ferric Redox Couple in the Acid Media. *Electrochim. Acta* 1974, 19, 607–610.
- (51) Hamelin, A.; Weaver, M. J. Metal Substrate Effects upon the Kinetics of Simple Electrochemical Reactions: The Reduction of Cobalt(III) Ammines at Single-Crystal Gold Faces. *J. Electroanal. Chem. Interfacial Electrochem.* 1986, 209, 109–124.
- (52) Sawant, T. V.; Mckone, J. R. Flow Battery Electroanalysis: Hydrodynamic Voltammetry of Aqueous Fe(III/II) Redox Couples at Polycrystalline Pt and Au. ACS Appl. Energy Mater. **2018**, *1*, 4743–4753.
- (53) Kresse, G.; Furthmüller, J. Efficient Iterative Schemes for Ab Initio Total-Energy Calculations Using a Plane-Wave Basis Set. *Phys. Rev. B* **1996**, *54*, 11169–11186.
- (54) Laio, A.; Parrinello, M. Escaping Free-Energy Minima. *Proc. Natl. Acad. Sci. U.S.A.* **2002**, 99, 12562–12566.
- (55) Iannuzzi, M.; Laio, A.; Parrinello, M. Efficient Exploration of Reactive Potential Energy Surfaces Using Car-Parrinello Molecular Dynamics. *Phys. Rev. Lett.* **2003**, *90*, No. 238302.
- (56) Holze, R.Table 5.1. Exchange Current Densities and Rate Constants in Aqueous Systems. In *Electrochemistry Electrochemical Thermodynamics and Kinetics*; Lechner, M. D., Ed.; Springer, 2007; pp 276–378
- (57) Scott, S. L. The Burden of Disproof. ACS Catal. **2019**, *9*, 4706–4708.
- (58) Nørskov, J. K.; Studt, F.; Abild-Pedersen, F.; Bligaard, T. Fundamental Concepts in Heterogeneous Catalysis; John Wiley & Sons, Inc.: New Jersey, 2014; pp 85–113.
- (59) Hammer, B.; Nørskov, J. K. Theoretical Surface Science and Catalysis—Calculations and Concepts. *Adv. Catal.* **1972**, *45*, 71–129.
- (60) Leonard, K. C.; Bard, A. J. Pattern Recognition Correlating Materials Properties of the Elements to Their Kinetics for the Hydrogen Evolution Reaction. J. Am. Chem. Soc. 2013, 135, 15885—15880
- (61) Greeley, J.; Nørskov, J. K.; Kibler, L. A.; El-Aziz, A. M.; Kolb, D. M. Hydrogen Evolution Over Bimetallic Systems: Understanding the Trends. *ChemPhysChem* **2006**, *7*, 1032–1035.
- (62) Lima, F. H. B.; Zhang, J.; Shao, M. H.; Sasaki, K.; Vukmirovic, M. B.; Ticianelli, E. A.; Adzic, R. R. Catalytic Activity-d-Band Center Correlation for the O2 Reduction Reaction on Platinum in Alkaline Solutions. *J. Phys. Chem. C* **2007**, *111*, 404–410.